Progress In Electromagnetics Research M, Vol. 102, 181–192, 2021

Metamaterial Vivaldi Printed Circuit Antenna Based Solar Panel for Self-Powered Wireless Systems

Ahmed Abdulmjeed[1], Taha A. Elwi[2, *], and Sefer Kurnaz[1]

Abstract—A high-gain wide-band planar antenna with H-Shaped Resonators (HSRs) for Self-Powered wireless systems is proposed in this paper. The proposed antenna consists of four major parts, namely, a grating Vivaldi electrical dipole, a half-ring magnetic dipole, HSRs, and a solar panel reflector. The dipoles are etched from both antenna substrate sides by each half on one side. The HSR structures are etched on a single side of the used substrate to avoid the capacitive coupling effects which cause the radiation efficiency reduction. HSR inclusions are designed and tested numerically to have the desired electromagnetic properties at frequency band of interest. After introducing the HSR inclusions to the antenna structure, the antenna performance is tested numerically and compared to that without HSR inclusions. The fabricated prototype based HSR structure shows an enhanced gain bandwidth product to cover the frequencies from 1.75 GHz up to 7.43 GHz with a gain varying from 9.52 dBi up to 16.71 dBi over the entire frequency range. Finally, an excellent agreement has been achieved between the gathered numerical results and those from the experimental measurements.

1. INTRODUCTION

Substantial developments have been conducted on the antenna design techniques to enhance their performance in terms of gain bandwidth products [1]. For example in [2], a microstrip antenna was invented by L-prop feed with a bandwidth of 36% and an average gain of approximately 7 dBi. A Vivaldi antenna with a bandwidth of 3.1 GHz to 10.6 GHz and a gain of approximately 6 dBi was developed [3].

In [4], a quasi-Yagi antenna that operated from 7.32 GHz to 11.15 GHz of a maximum gain of 8.6 dBi was proposed. Elwi et al. [4] designed a complementary antenna by exciting electric and magnetic dipoles; this antenna was revealed to provide reliable gain stability with low back radiation of a wide bandwidth. Several designs in [5–7] were developed from different Vivaldi antennas such as spiral loops, magnetic dipoles, H-shaped resonators, and loop-dipole composites. However, these antennas suffered from low and unstable gain performance. Therefore, the introduction of metamaterial structures to the antenna designs has become common because of their unique electromagnetic properties [8], such as low or zero refractive indexes which control the antenna radiation [9]. Abdul Hassain et al. [10] introduced a microstrip antenna with zero refractive index metamaterials in the substrate, which improved the gain by 1 dB to 2 dB. However, this type of inclusions may increase the antenna size and profile.

In this paper, a grating Vivaldi antenna based on electrical and magnetic dipoles, inspired from the antenna structure in [6] with several modifications to enhance the antenna performance, is proposed. A microstrip to coplanar stripline is replaced with a symmetrical microstrip to stripline transition balun to achieve broad bandwidth impedance. Five rows of HSR are implemented to improve the antenna gain. Grating Vivaldi antenna is used instead of Vivaldi antenna to further increase the antenna gain. Finally, the proposed antenna structure is fabricated then measured.

Received 24 March 2021, Accepted 6 May 2021, Scheduled 26 May 2021

* Corresponding author: Taha A. Elwi (taelwi82@gmail.com).

[1] Altinbas University, Mahmutbey Dilmenler Caddesi, No: 26, Bağcılar 34217, Istanbu. [2] Department of Electronics and Communication, Al-Mammon University College, Baghdad, Iraq.

2. ANTENNA DESIGN

The proposed antenna structure is mounted on an FR4 substrate, with 1.6 mm thickness, $\varepsilon_r = 4.6$, and $\tan\delta = 0.0004$. The substrate layer is designed to be embedded in parallel to the antenna parts as shown in Fig. 1. The antenna consists of four major parts: a grating Vivaldi electric dipole, a magnetic half-loop dipole, a microstrip-to-stripline transition balun, and HSR inclusions. The magnetic dipole structure is adopted from the antenna design presented in [6], and HSR design is inspired from [11]. The antenna is excited with an SMA connector to be soldered to the balun. To achieve a broadband impedance matching, the SMA inner part is connected to strip line, and the SMA outer part is soldered to the ground plane [12] as shown in Fig. 1. The grating Vivaldi antenna consists of three segments attached to the magnetic dipole as seen in Fig. 1. Such a combination is to achieve Huygens source [13]; when the electric and magnetic dipoles are excited with the same amplitude and phase, it realizes a wide band leakage [14]. Therefore, the interference between the radiation fringing of the magnetic dipole, $\lambda/1$ length, and the electrical dipole, $\lambda/2$ length, could realize unidirectional radiation patterns [15]. Moreover, the distance between the electrical dipole and magnetic dipole is altered to achieve 90° phase difference that generates a TEM mode [16]. However, a scattering in the generated beam could occur due to the edges of the grating Vivaldi antenna which degrades the antenna gain [17]. Therefore, an HSR array is introduced to enhance the antenna radiation efficiency by matching the electromagnetic antenna aperture impedance to the free space intrinsic impedance [15]. It is good to mention that the technology of HSR has already been presented in different publications such as [15]; however, the main innovation for its use in this work is to enhance matching between the proposed antenna and the circuit rectifier. The basic antenna structure of the proposed work shows a significant variation in the real part of the relative matching impedance, which reduces the matching between the proposed antenna and the rectifier circuit. Therefore, the introduction of the proposed HSR positively affects the matching impedance between the proposed antenna structure and the RF harvesting board as will be seen later. Moreover, the proposed HSR geometry is applied in this design to increase the radiation efficiency which

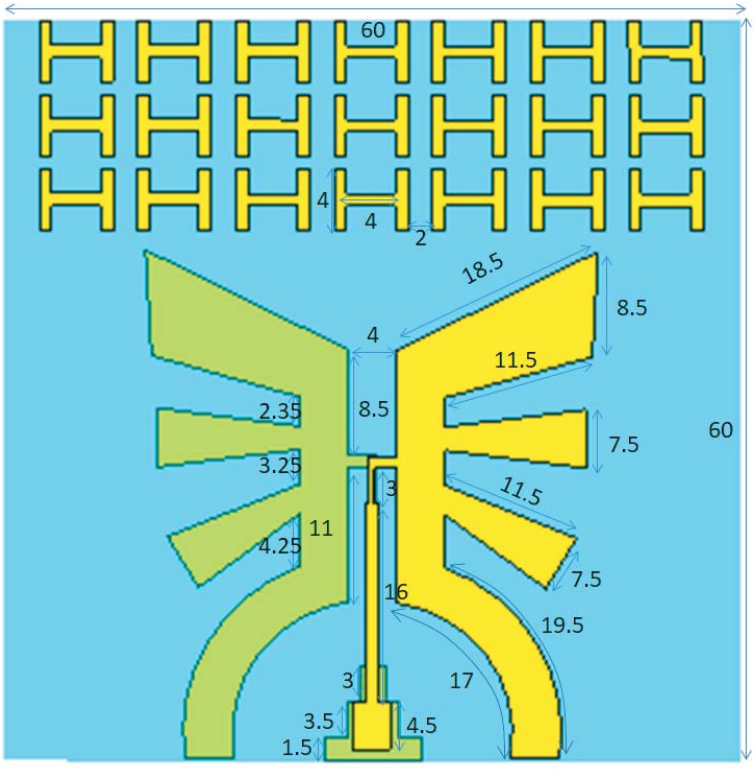

Figure 1. Configuration of the proposed antenna.

in return increases the antenna gain to enhance the electromagnetic rectification efficiency, i.e., increase the harvested voltage. All the related results in terms of rectification efficiency with the impedance spectra before and after adding the proposed HSR structures are discussed later.

3. DESIGN METHODOLOGY

3.1. Antenna Performance without HSR

Numerically, the antenna performance is explored in this section before introducing HSR in terms of S_{11} and radiation patterns at 2.45 GHz and 5.8 GHz at Wi-Fi bands. The numerical analysis is performed by invoking Finite Integral Technique (FIT) based on CST MWS formulation [18]. The presented S_{11} spectrum in Fig. 2(a) indicates that the antenna, without HSR inclusions, shows a wideband; however, in Figs. 2(b) and 2(c) an obvious deterioration is found in the antenna gain due to the surface wave leakage.

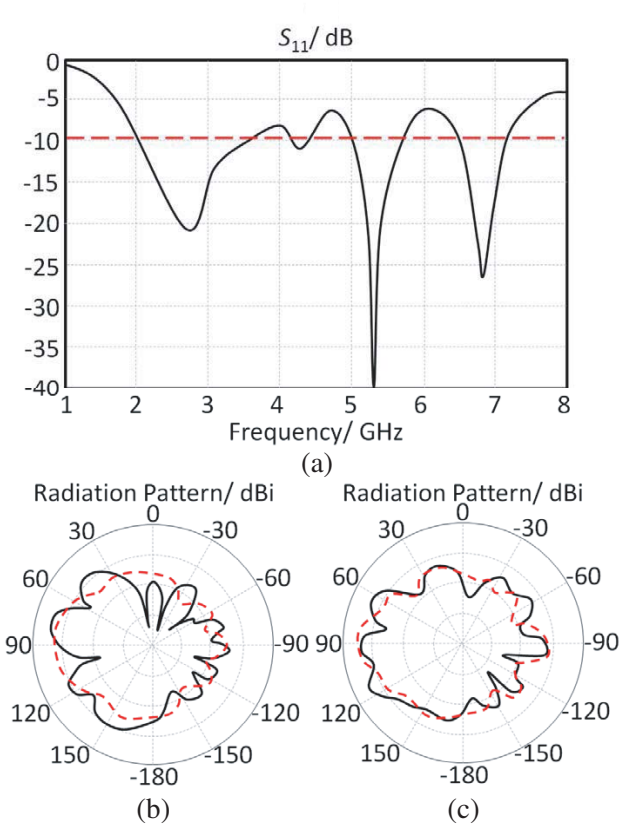

Figure 2. Simulated results of the antenna without HSR inclusions: (a) S_{11} spectrum, (b) and (c) radiation patterns at 2.45 GHz and 5.8 GHz, previously.

3.2. HSR Design

The proposed HSR unit cell is characterized through retrieving the relative refractive index from the simulated S-parameters. The retrieving process is performed using a robust method that was discussed in [16–18]. The unit cell is centered inside a factious waveguide (see Fig. 3), to evaluate the S-parameters. Therefore, the boundary conditions are assigned as a perfect electric conductor along the x-axis and a perfect magnetic conductor along the z-axis.

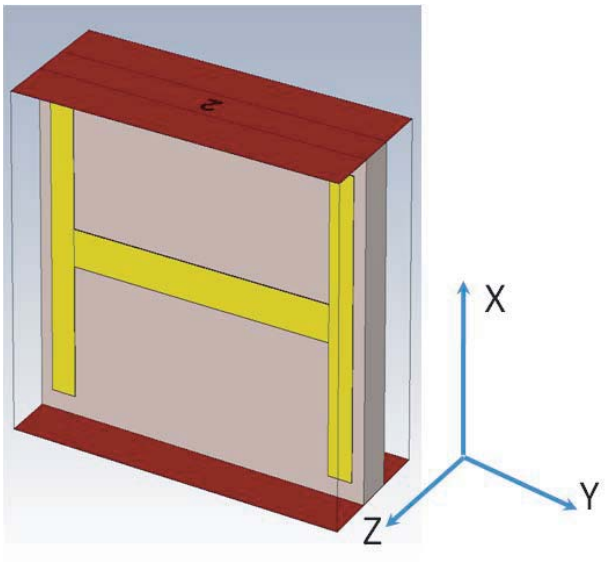

Figure 3. HSR unit cell inside the factious waveguide.

It is found that the proposed HSR provides a refractive index (n), see Fig. 4, a variation between 0 and 3. Therefore, such a unit cell can be applied to the antenna structure to focus the radiation pattern in the end-fire direction.

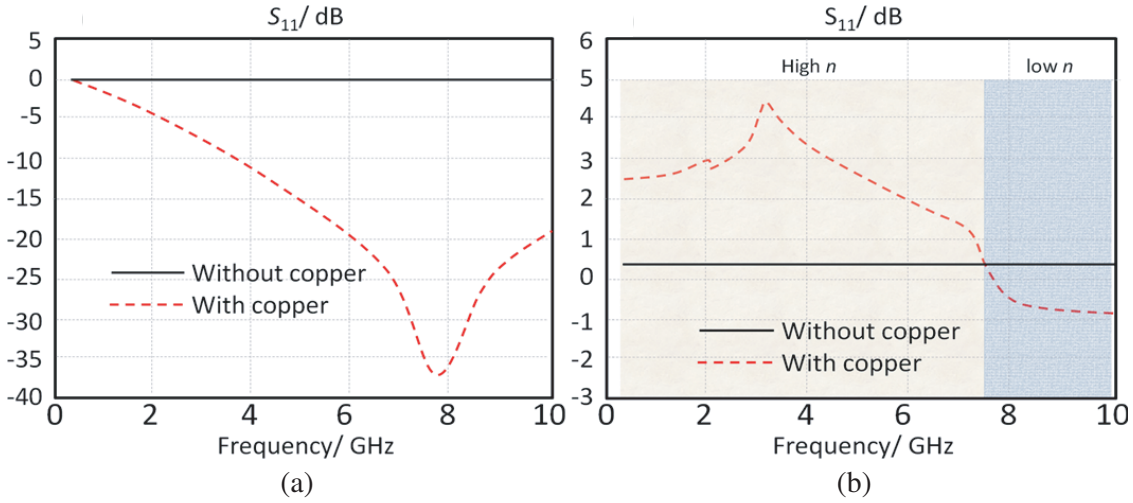

Figure 4. Characterizations of the HSR unite cell: (a) S_{11} and (b) retrieved refractive index.

3.3. Antenna Performance Based HSR Inclusions

According to Snell's law, $n_i \sin\theta_i = n_t \sin\theta_t$, i refers to the incident wave and t to the transmitted wave, when the refractive index value of the substrate layer (n_i) becomes large enough, with a certain incident angle (θ_i), and the diffracted angle (θ_t) becomes large at small reflective index of the HSR layer (θ_t). Consequently, the energy aggregates beam focusing, which leads to high gain in such a direction. The HSR layer provides higher n from the substrate n to focus the radiation to the end-fire. This layer consists of three rows and seven columns of HSR unit cells to be mounted on the top side of the substrate. The performances of the antenna with HSR inclusions in terms of S_{11} spectrum and radiation patterns are presented in Fig. 5.

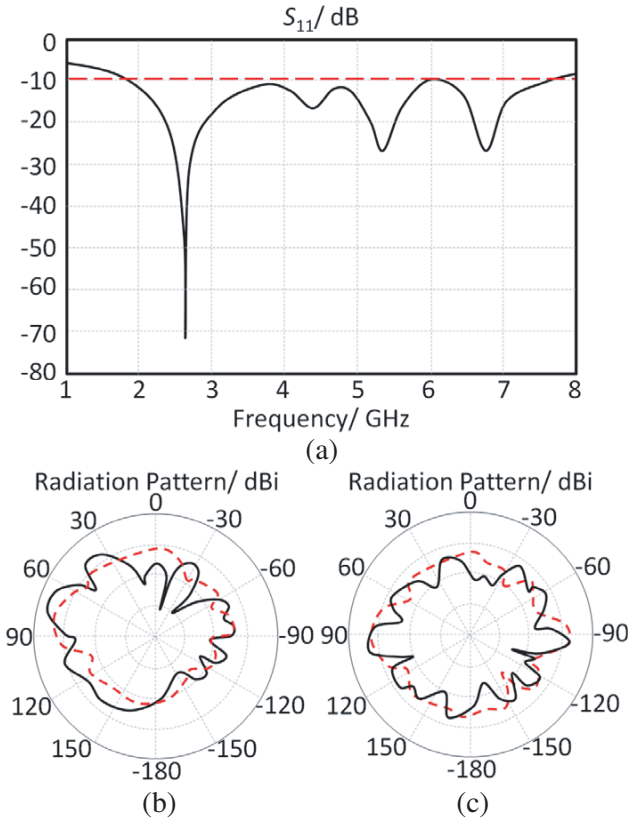

Figure 5. Simulated results of the antenna with HSR: (a) S_{11} spectrum, (b) and (c) radiation patterns at 2.45 GHz and 5.8 GHz, respectively. Note: The red line for the YX-plane and the black line for the YZ-plane from the CSTMWS.

4. MEASUREMENTS AND VALIDATIONS

4.1. Antenna Design Validation

In this section, the obtained numerical results in Fig. 5, S_{11} spectrum and radiation patterns, are validated numerically using HFSS [19]. The regarded results from CST MWS and HFSS simulations are gathered in Fig. 6. The results of the radiations pattern indicate that the beam is highly focused when HSR is employed. An excellent matching has been observed between the results of the used software packages.

4.2. Antenna Measurements and Discussions

As shown Fig. 7, the fabricated prototype is presented. The antenna performance is measured with HSR structure to get good agreements with the simulation results. The measured S_{11} spectrum is obtained from Anritsu 37347D Network Analyzer (VNA). The radiation patterns are measured inside an RF chamber with a dual-polarized horn antenna (LB-SJ-20180), an N9030A PXA signal analyzer, and a signal generator.

The proposed antenna based HSR structure is found to show an end-fire direction 2.45 GHz and 5.8 GHz as depicted in Fig. 8. The antenna provides a bandwidth from 1.75 GHz up to 7.43 GHz. Nevertheless, the antenna gain is found to be approximately 9.5 dBi and up to 13 dBi at 2.45 GHz and 5.8 GHz, respectively.

Figure 9 shows the current distributions for the antennas with and without the HSR structures. The antenna based on HSR inclusions contributes the current movement to end of the patch, thereby

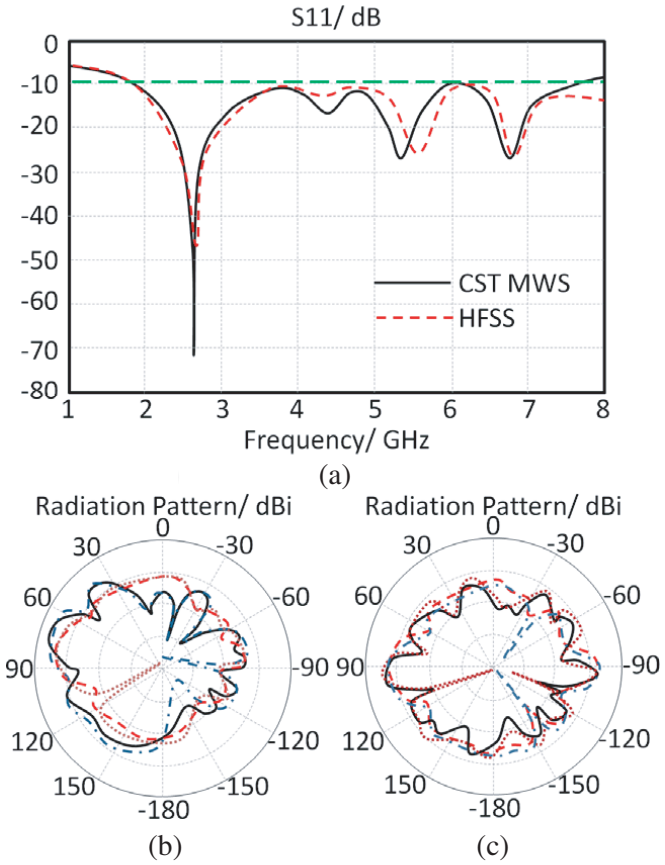

Figure 6. Simulated results of the antenna with HSR: (a) S_{11} spectrum, (b) and (c) radiation patterns at 2.45 GHz and 5.8 GHz, respectively. Note: The red line for the YX-plane and the black line for the YZ-plane from the CSTMWS. The brown line for the YX-plane and the blue line for the YZ-plane from HFSS.

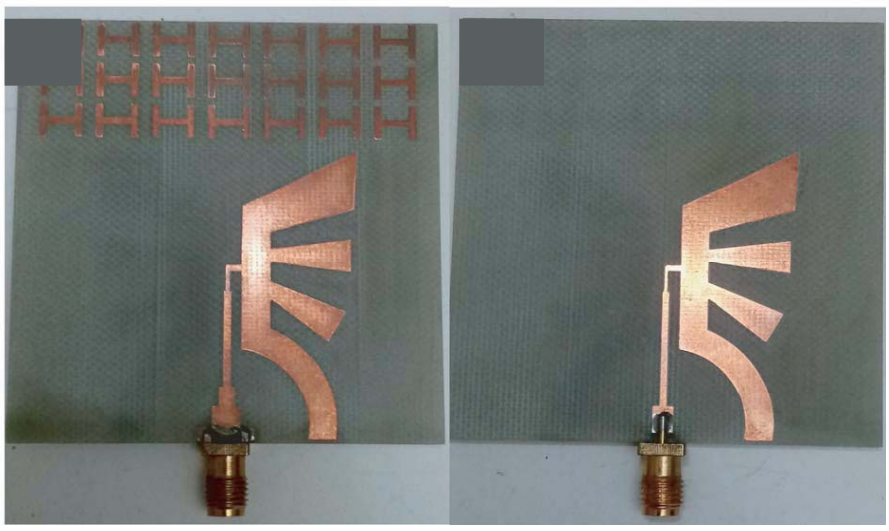

Figure 7. Fabricated antenna prototype: (a) back view and (b) front view.

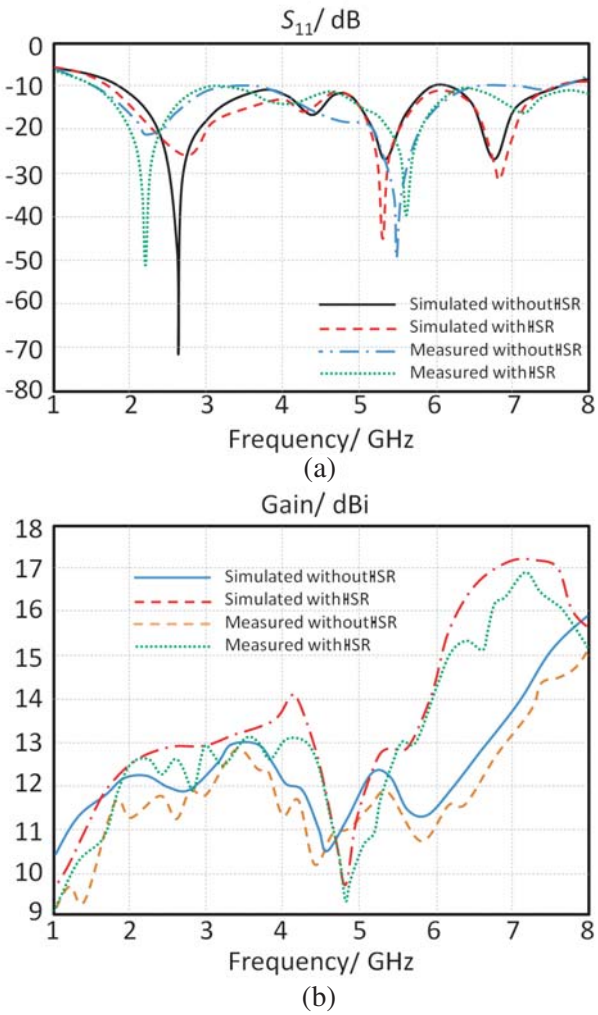

Figure 8. Simulated and measured antenna performance: (a) S_{11} and (b) gain spectra.

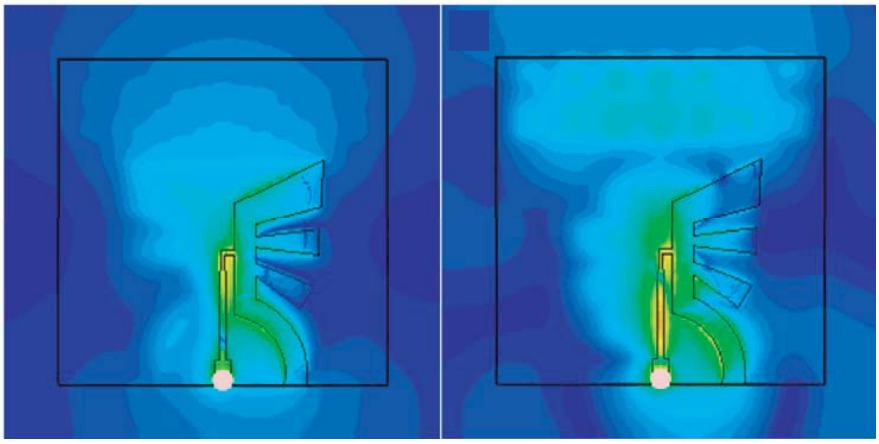

Figure 9. Current distribution of both antennas: (a) without HSR and (b) with HSR structures.

Table 1. Comparison between the achieved results other published results.

Reference	Dimensions (mm^2)	Bandwidth (GHz)	Max. Gain (dBi)
[1]	36×28	2.1 GHz–10 GHz	4.3
[4]	44×30	1.6 GHz–8.5 GHz	5.1
[5]	34×32	3.1 GHz–10 GHz	3.7
[7]	39×38	3 GHz–10 GHz	4.4
[11]	40×35	2 GHz–10 GHz	4.7
[15]	70×70	3 GHz–12 GHz	5.5
[16]	50×63	4.2 GHz–6 GHz	3.5
[20]	92.5×133	5.5 GHz–6 GHz	10
[21]	185×172	6.52 GHz–6.73 GHz	15.1
Proposed antenna	60×60	1.75 GHz–7.43 GHz	16.71

enhancing gain in the end-fire. The most common and effective way to extract the parameters of metamaterial inclusions was employed in [17].

Table 1 presents a comparison between the proposed antenna performances with respect to other published results in the literature.

By comparing the proposed antenna with all previous listed references, it is obvious that the proposed antenna shows a higher gain with maximum size reduction over a wide bandwidth than the published relative work. This makes the proposed antenna a good competitor to other published results in the literature.

5. SOLAR PANEL INTEGRATION TO THE PROPOSED ANTENNA STRUCTURE

In this section, the effects of introducing a solar panel as a reflector structure, see Fig. 10(a), on the proposed antenna performance are discussed in terms of S_{11} and gain spectra. As seen in Figs. 10(b) and 10(c), the S_{11} and gain spectra of proposed antenna are compared against the antenna performance with the solar panel reflector experimentally. It is found that the proposed antenna based on the solar panel reflector shows insignificant changes in the S_{11} spectra as depicted in Fig. 10(b). However, the gain is improved about 2 dBi as seen in the gain spectra in Fig. 10(c) over the frequency band of interest. Such a gain increase is attributed to the metal bus-bar solar panel ground plane, see Fig. 10(a), and effects of the solar panel on the antenna back radiation reflection [7]. Therefore, there are no effects of the antenna on the solar panel performance. However, the solar panel increases the antenna gain slightly because of the reflection of antenna back radiation from the solar panel ground plane. The back panel of solar cell is covered with a conductive shield to ensure all radiation reflected away from the solar panel as shown in Fig. 10(a).

It is good to mention that the proposed antenna is mounted on a rotating arm inside an RF anechoic chamber to measure the radiation patterns. The measurement setup consists of a transmitting horn antenna with a focusing lens that is connected to Professional Network Analyzer (Agilent PNA 8720) on port 1. The proposed antenna is connected to the other port of the used PNA instrument. The antennas are separated with 4 m long distance to ensure the far-field region. This setup is used to perform radiation patterns and gain spectra measurements. However, the S_{11} spectra are recorded directly on the PNA on port 1 without the need for the second port connection.

On the other hand, as mentioned later, the proposed HSR structure array is conducted to the proposed study to maintain the matching impedance mostly constant around 50 Ω, see Fig. 11(a), in the real part and around 0 Ω for the imaginary part as shown in Fig. 11(b). Nevertheless, the use of the proposed HSR supports the antenna radiation efficiency to be almost stable over a wide range of frequencies as seen in Fig. 11(c).

It can be obviously noticed that the material losses of the proposed solar panel have no significant effects on the antenna efficiency because the antenna is located perpendicular to the solar panel which

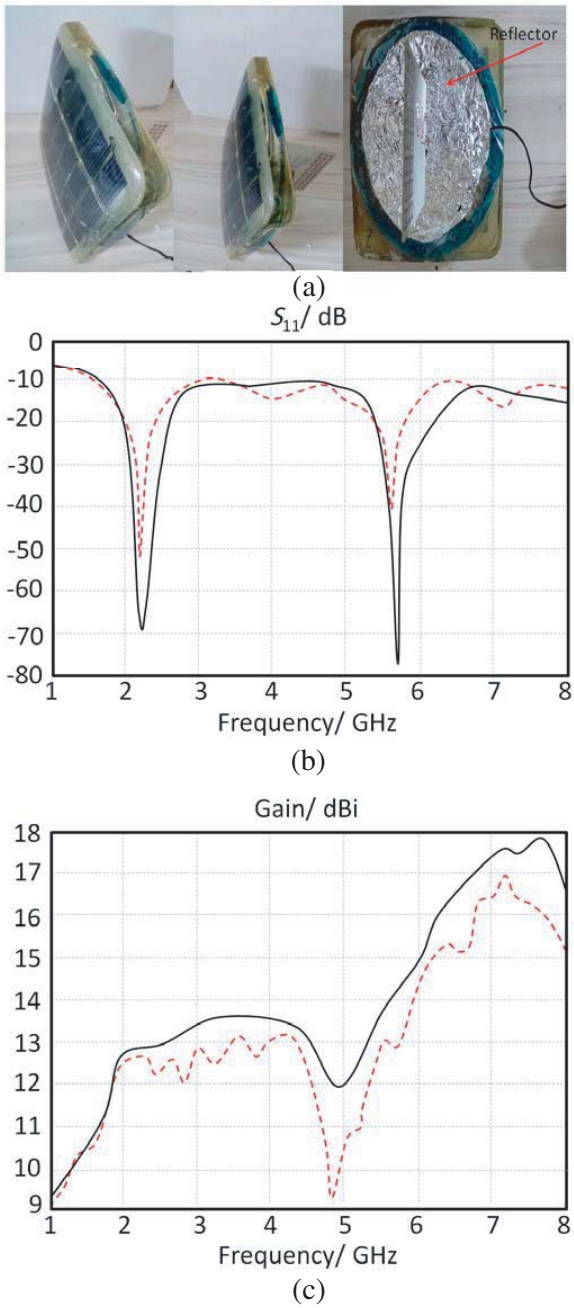

Figure 10. Antenna performance based on solar panel reflector: (a) Antenna structure with the solar pane, (b) S_{11} spectra, and (c) gain spectra. **Note:** Red color dotted line is the measurements without solar panel. The black solid line is the measurements with solar panel.

maintains the antenna radiation away from the solar panel.

Now, the solar panel I-V characteristics are measured after the introduction of proposed antenna. Comparison is conducted to realize the effects of the antenna introduction on the considered solar panel. Therefore, it is found that insignificant effects are found on the solar panel performance, see Fig. 12, after and before the antenna introduction. This is due to having the antenna structure on the back panel of the solar panel. In those measurements, the solar energy is characterized in the photo-current and photo-voltage diagram at different light intensities by changing the value from 500 $\mathrm{W/m^2}$ to 1000 $\mathrm{W/m^2}$ as presented in Fig. 12.

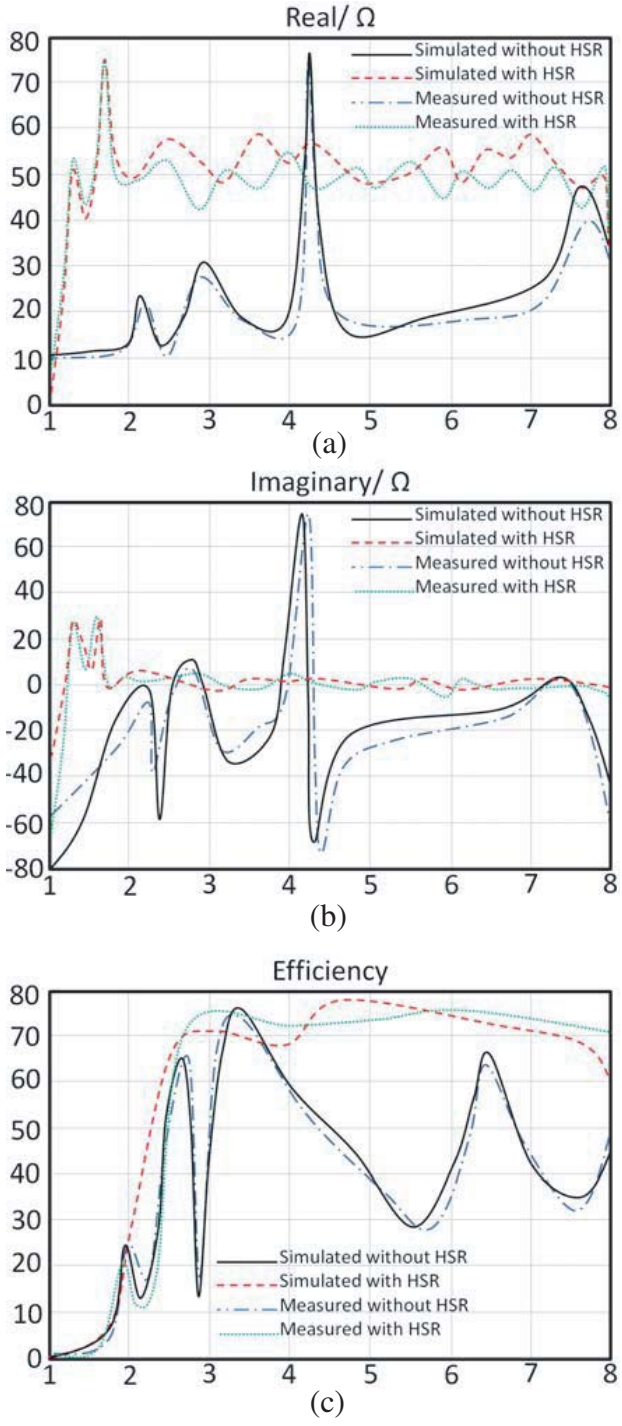

Figure 11. Antenna performance with and without the proposed HSR: (a) real part of the impedance, (b) imaginary part of the impedance, (c) radiation efficiency spectra.

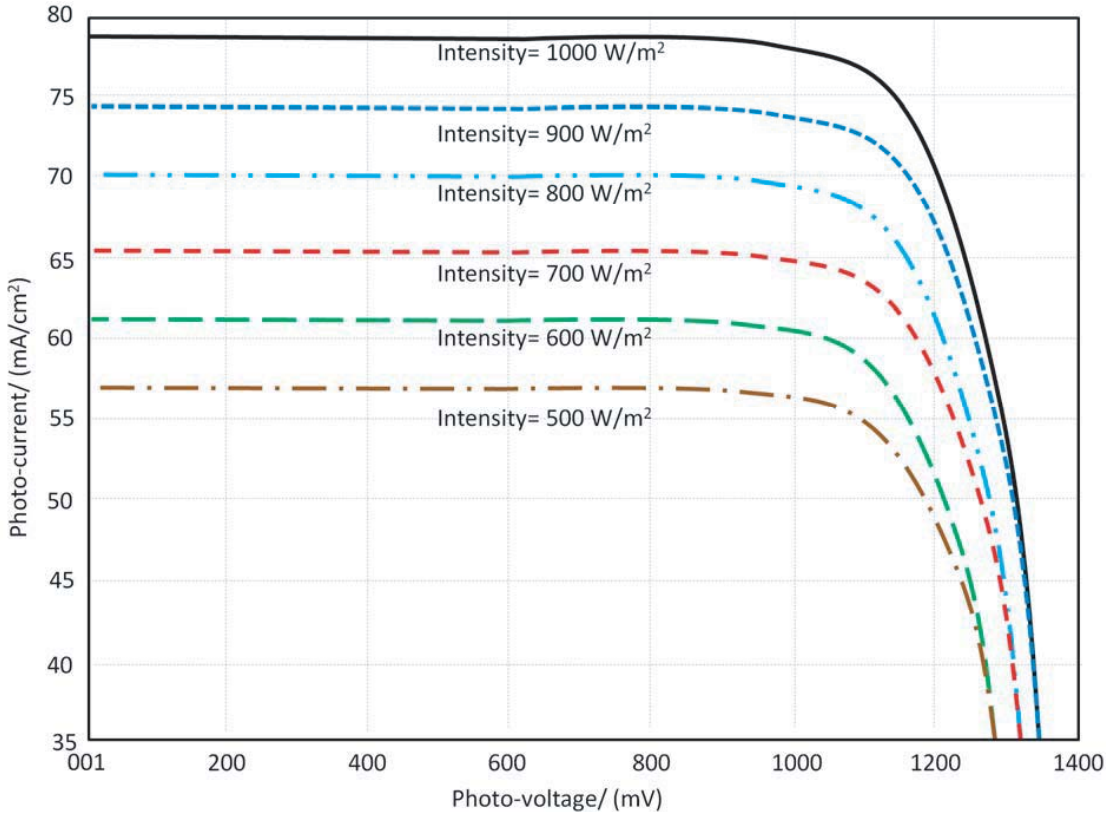

Figure 12. Solar panel performance after introducing the proposed antenna structure at the back panel.

6. CONCLUSION

A high gain broadband microstrip antenna with HSR inclusions is demonstrated in this paper for self-powered wireless systems in the Wi-Fi bands. A broadband is achieved by using microstrip-to-stripline transition balun to match the antenna bandwidth, $|S_{11}| < -10$ dB, from 1.75 GHz up to 7.43 GHz. The proposed antenna shows a significant enhancement in the gain between 9.52 dBi and 16.71 dBi. Such gain enhancement is attributed to the introduction of HSR array. When the proposed antenna is compared to other published results in the literature, it is found that the proposed antenna provides remarkable enhancements in terms of gain, bandwidth, and size reduction. On the other hand, the proposed antenna performance is measured when it is mounted on a solar panel as a reflector. It is found that the antenna performance in terms of S_{11} spectra has not affected; however, the antenna gain is enhanced in general over the frequency band of interest. The performance of used solar panel is measured in terms of I-V characteristics to show no effects on the solar energy harvesting, because the antenna structure is attached on the back panel of the solar energy. Finally, an excellent agreement has been achieved between simulated and measured results.

REFERENCES

1. Elwi, T. A., "A further realization of a flexible metamaterial-based antenna on nickel oxide polymerized palm fiber substrates for RF energy harvesting," *Wireless Personal Communications*, Vol. 10, No. 12, 1–15, August 2020,
2. Alnaiemy, Y., T. A, Elwi, and L. Nagy, "An end fire printed monopole antenna based on electromagnetic band gap structure," *Automatika*, Vol. 61, No. 3, 482–495.

3. Elwi, T. A., "Remotely controlled reconfigurable antenna for modern applications," *Microwave and Optical Letters*, Vol. 6, No. 1, 1–19, April 2020,
4. Elwi, T. A., "Further investigation on solant-rectenna based flexible Hilbert-shaped metamaterials," *IET Nanodielectrics*, Vol. 4, No. 12, 1–12, March 2020.
5. Elwi, T. A. and A. M. Al-Saegh, "Further realization of a flexible metamaterial based antenna on indium nickel oxide polymerized palm fiber substrates for RF energy harvesting," *International Journal of Microwave and Wireless Technologies*, Vol. 5, No. 4, 1–9, Cambridge, May 2020,
6. Al-Dulaimi, Z., T. A. Elwi, and D. C. Atilla, "Design of a meander line monopole antenna array based Hilbert-shaped reject band structure for MIMO applications," *IETE Journal of Research*, Vol. 66, No. 1, 1–10, March 2020,
7. Elwi, T. A., D. A. Jassim, and H. H. Mohammed, "Novel miniaturized folded UWB microstrip antenna-based metamaterial for RF energy harvesting," *International Journal of Communication Systems*, Vol. 1, No. 2, January 2020,
8. Alnaiemy, Y., T. A. Elwi, and L. Nagy, "Mutual coupling reduction in patch antenna array based on EBG structure for MIMO applications," *Periodica Polytechnica Electrical Engineering and Computer Science*, Vol. 1, No. 4, 1–11, September 2019,
9. Al-Sabbagh, H. M., T. A. Elwi, Y. Al-Naiemy, and H. M. Al-Rizzo, "A compact triple-band metamaterial-inspired antenna for wearable applications," *Microwave and Optical Technology Letters*, Vol. 11, No. 2, October 2019.
10. Abdul Hassain, Z. A., A. R. Azeez, M. M. Ali, and T. A. Elwi, "A modified compact bi-directional UWB tapered slot antenna with double band-notch characteristics," *Advanced Electromagnetics*, Vol. 8, No. 4, September 2019.
11. Elwi, T. A., Z. A. AL-Hussain, and O. Tawfeeq, "Hilbert metamaterial printed antenna based on organic substrates for energy harvesting," *IET Microwaves, Antennas & Propagation*, Vol. 12, No. 4, 1–8, June 2019.
12. Ahmed, H. S. and T. A. Elwi, "On the design of a reject band filter for antennas mutual coupling reduction," *International Journal of RF and Microwave Computer-Aided Engineering*, Vol. 11, No. 3, 1–11, April 2019,
13. Elwi, T. A., "Printed microwave metamaterial-antenna circuitries on nickel oxide polymerized palm fiber substrates," *Nature Scientific Reports*, Vol. 9, No. 2174, 1–14, January 2019.
14. Elwi, T. A., "Novel UWB printed metamaterial microstrip antenna based organic substrates for RF-energy harvesting applications," *AEU — International Journal of Electronics and Communications*, Vol. 101, 1–10, January 2019.
15. Wang, H., S.-F. Liu, L. Chen, W.-T. Li, and X.-W. Shi, "Gain enhancement for a broadband vertical planar printed antenna with H-shaped resonator structures," *IEEE Trans. Antennas Propag.*, Vol. 62, 4411–4415, 2014.
16. El-Nady, S., H. M. Zamel, M. Hendy, A. A. Zekry, and A. Attiya, "Gain enhancement of a millimeter wave antipodal vivaldi antenna by epsilon-near-zero metamaterial," *Progress In Electromagnetics Research C*, Vol. 85, 105–116, 2018.
17. Elwi, T. A. and B. A. Ahmed, "A fractal metamaterial based printed dipoles on a nickel oxide polymer palm fiber substrate for Wi-Fi applications," *AEU — International Journal of Electronics and Communications*, Vol. 96, 122–129, September 2018.
18. www.cst.com.
19. www.ansys.com.
20. Jiang, Z. H., Q. Wu, D. E. Brocker, P. E. Sieber, and D. H. Werner, "A low-profile high-gain substrate-integrated waveguide slot antenna enabled by an ultrathin anisotropic zero-index metamaterial coating," *IEEE Transactions on Antennas and Propagation*, Vol. 62, 1173–1184, 2014.
21. Cheng, H. Z., X. Liu, X. Huo, and K. Fan, "Planar high gain circularly polarized element antenna for array applications," *IEEE Transactions on Antennas and Propagation*, Vol. 63, No. 5, 1–1, May 2015.